



PCCP

### Molecular Origins of Bulk Viscosity in Liquid Water.

Journal:	<i>Physical Chemistry Chemical Physics</i>
Manuscript ID	CP-ART-03-2020-001560
Article Type:	Paper
Date Submitted by the Author:	22-Mar-2020
Complete List of Authors:	<p>Yahya, Ahmad; University of Cincinnati, CEAS - Chemical &amp; Env Eng            Tan, Luoxi; University of Cincinnati, CEAS - Chemical &amp; Env Eng            Perticaroli, Stefania; Oak Ridge National Laboratory, Joint Institute for Neutron Sciences            Mamontov, Eugene; Oak Ridge National Laboratory, Spallation Neutron Source            Pajerowski, Daniel; Oak Ridge National Laboratory            Neufeind, Joerg; Oak Ridge National Laboratory, Spallation Neutron Source            Ehlers, Georg; Oak Ridge National Laboratory, Quantum Condensed Matter Division            Nickels, Jonathan; University of Cincinnati, CEAS - Chemical &amp; Env Eng</p>

SCHOLARONE™  
Manuscripts

## ARTICLE

## Molecular Origins of Bulk Viscosity in Liquid Water.

Ahmad Yahya<sup>a</sup>, Luoxi Tan<sup>a</sup>, Stefania Perticaroli<sup>b</sup>, Eugene Mamontov<sup>c</sup>, Daniel Pajeroski<sup>c</sup>, Joerg Neufeind<sup>c</sup>, Georg Ehlers<sup>c</sup>, Jonathan D. Nickels<sup>a\*</sup>.

Received 00th January 20xx,  
Accepted 00th January 20xx

DOI: 10.1039/x0xx00000x

The rapid equilibrium fluctuations of water molecules are intimately connected to the rheological response; molecular motions resetting the local structure and stresses seen as flow and volume changes. In the case of water or hydrogen bonding liquids generally, the relationship is a non-trivial consideration due to strong directional interactions complicating theoretical models and necessitating clear observation of the timescale and nature of the associated equilibrium motions. Recent work has illustrated a coincidence of timescales for short range sub-picosecond motions and the implied timescale for the shear viscosity response in liquid water. Here, neutron and light scattering methods are used to experimentally illustrate the timescale of bulk viscosity and provide a description of the associated molecular relaxation. Brillouin scattering has been used to establish the timescale of bulk viscosity; and borrowing the Maxwell approach, the ratio of the bulk viscosity,  $\zeta$ , to the bulk modulus,  $K$ , yields a relaxation time,  $\tau_b$ , which emerges on the order of 1-2 ps in the 280K to 303K temperature range. Inelastic neutron scattering is subsequently used to describe the motions of water and heavy water at the molecular scale, providing both coherent and incoherent scattering data. A rotational (alternatively described as localized) motion of water protons on the 1-2 ps timescale is apparent in the incoherent scattering spectra of water, while the coherent spectra from D2O on the length scale of the first sharp diffraction peak, describing the microscopic density fluctuations of water, confirms the relaxation of water structure at a comparable timescale of 1-2 ps. The coincidence of these three timescales provides a mechanistic description of the bulk viscous response, with the local structure resetting due to rotational/localized motions on the order of 1-2 ps, approximately three times slower than the relaxations associated with shear viscosity. In this way we show that the shear viscous response is most closely associated with changes in water network connectivity, while the bulk viscous response is associated with local density fluctuations.

## Introduction

Water is perhaps the most important and intriguing molecule in the human experience. Important because of its ubiquitous presence in daily life, its role as solvent and reagent in biology and industrial applications, and as a vital environmental resource. Intriguing because of the complex way that structure and hydrogen bonding (HB) combine to produce a rich phase diagram<sup>8, 9</sup> and anomalous physical properties<sup>10-12</sup> (especially near surfaces). We call the properties of water anomalous because models and theoretical frameworks<sup>10, 13-16</sup> which exist to predict local structure, dynamics, macroscopic transport and thermodynamic properties for monoatomic liquids<sup>17-21</sup> and Lennard-Jones fluids<sup>22-24</sup>, struggle to predict properties of water accurately. This is due to the local ordering of the molecules and dynamical complexity introduced by electrostatic and HB interactions, including vibrational, rotational, and translational

components<sup>3, 25</sup> of molecular motions, along with the kinetics of the HB itself<sup>25</sup>.

Viscosity is a property of water describing resistance to flow, and it emerges directly from the propensity of the molecules to move and reorganize the local structure on the molecular scale. On the human scale a relationship can be expressed quantitatively as a pair of coefficients relating stress to the rate of strain in the generalized form of Newton's law of viscosity<sup>26</sup>;

$$\sigma_{ij} = \mu \left( \frac{\partial v_j}{\partial x_i} + \frac{\partial v_i}{\partial x_j} \right) + \left( \frac{2}{3}\mu - \zeta \right) \left( \frac{\partial v_x}{\partial x_x} + \frac{\partial v_y}{\partial x_y} + \frac{\partial v_z}{\partial x_z} \right) \delta_{ij} \quad (1).$$

Here,  $\sigma_{ij}$  is the stress tensor, and  $v$  is the velocity tensor, both which are a function of the Cartesian coordinates  $x$ ,  $y$ , and  $z$ .  $\delta_{ij}$  is the unit tensor. The two coefficients,  $\mu$  and  $\zeta$ , are the shear viscosity and bulk viscosity respectively. The bulk viscosity is alternately referred to as the volume viscosity or dilatational viscosity; reflecting the viscous resistance to volume change.

The notion that a characteristic internal (molecular) relaxation time determines the viscosity of a liquid is quite old. Maxwell<sup>27</sup> proposed the concept, recognizing a fundamental molecular relaxation time,  $\tau_M$ , emerges as the ratio of shear viscosity,  $\mu$ , to infinite shear modulus,  $G_\infty$ . This relationship distinguishes the timescales at which the mechanical response of a liquid will be solid-like ( $\tau < \tau_M$ ) or liquid-like ( $\tau > \tau_M$ ). As nicely articulated in a recent review<sup>28</sup> of dynamics in liquids; the molecular scale origin of shear viscosity emerges from the timescale of the shear stress correlations within the liquid. This Maxwell relaxation time,  $\tau_M$ , can be expressed using the Green-Kubo

<sup>a</sup>Department of Chemical and Environmental, Engineering, University of Cincinnati, Cincinnati, OH.

<sup>b</sup>Shull Wollan Center — a Joint Institute for Neutron Sciences, Oak Ridge National Laboratory, Oak Ridge, Tennessee, United States

<sup>c</sup>Neutron Scattering Division, Oak Ridge National Laboratory, Oak Ridge, Tennessee, United States

\*Corresponding Author — Jonathan D. Nickels, University of Cincinnati, 2901 Woodside Drive. PO Box 210012. Cincinnati OH 45221. Email: jonathan.nickels@uc.edu.

approach within the fluctuation-dissipation theorem<sup>29, 30</sup>, formulated as;

dynamics of water/heavy water on length scales from approximately 3 Å to 3 nm and timescales from the nanosecond

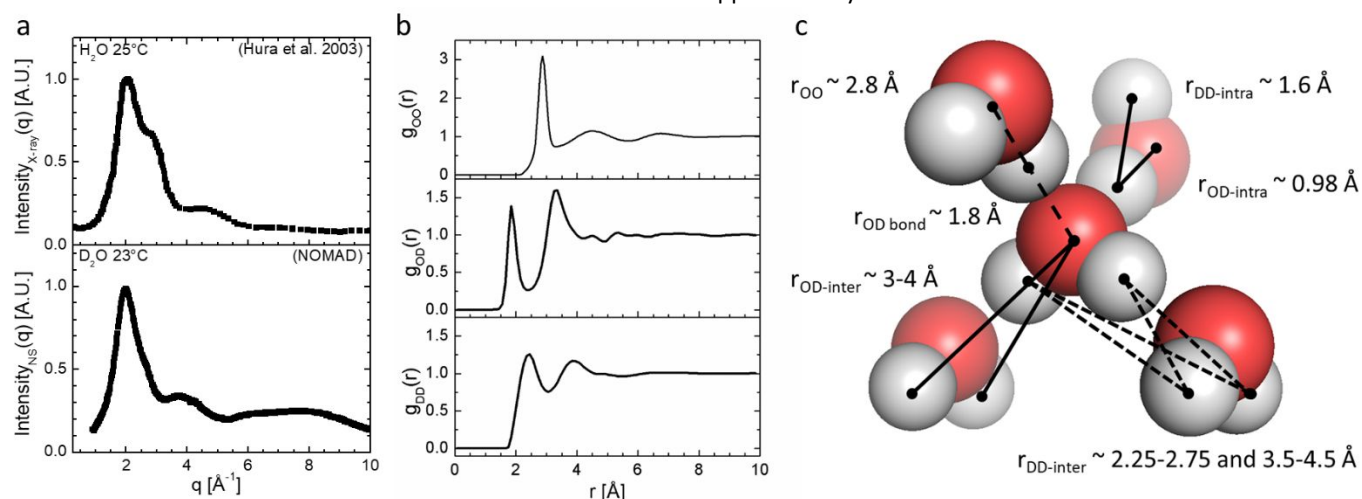


**Figure 1.** Water average structure. **(a)** X-ray (XRD)<sup>1</sup> and neutron (ND) diffraction data from liquid water (X-ray at 25°C, ND at 23°C). **(b)** Pair distribution functions for atoms pairs in H<sub>2</sub>O for liquid water at 25°C from Soper and Williams<sup>4</sup>. **(c)** Scattering data has contributed to the structural understanding of liquid water, shown here with approximate atomic pair distances annotated<sup>1, 4-7</sup>.  $r_{OOa}$  denotes O-O spacing within the first neighboring shell, while  $r_{OOb}$  denotes the second shell. where  $V$  is the macroscopic volume,  $\Omega_i$  is the molecular volume, and  $\sigma_{xy}(k)$  is the shear stress of the  $k^{\text{th}}$  molecule

$$\tau_M = \int_0^\infty \frac{\langle \sigma_{xy}(0) \sigma_{xy}(t) \rangle}{\langle (\sigma_{xy}(0))^2 \rangle} dt \quad (2),$$

where  $\sigma_{xy}(t)$  is the shear stress at time,  $t$ . This macroscopic conceptualization over generic volume,  $V$ , can in turn be connected to the molecular scale via the relation;

$$V\sigma_{xy} = \sum_i \Omega_i \sigma_{xy} \quad (3),$$

in this way, the molecular shear stress is connected to the local molecular configuration<sup>31</sup>, and we can conceive that molecular rearrangements reset local correlations in the shear stress.

Borrowing the approach for the shear viscosity, Hall<sup>32</sup> uses the ratio of  $\zeta$  to the bulk modulus,  $K$ , to yield a relaxation time,  $\tau_B$ , of the bulk viscous response. This timescale is obtained experimentally here using Brillouin scattering to establish the timescale of fundamental bulk viscosity relaxation time at 1-2 ps. Inelastic neutron scattering measurements show the motions of water and heavy water at the molecular length scale and the nanosecond to picosecond timescale. The individual molecular motions seen via incoherent scattering of H<sub>2</sub>O are well-described as a coupled translation/rotation mechanism; the rotational component of which also is observed around 2 ps. Coherent scattering of D<sub>2</sub>O reveals an ~2ps timescale associated with the lifetime of the intermolecular correlations comprising the first sharp diffraction peak. The coincidence of timescales suggests a mechanistic description of coordinated rotational motions allowing structural reorganization as the equilibrium motions responsible for bulk viscosity in liquid water.

## Results and Discussion

Both the local molecular configuration and the lifetime of local molecular correlations<sup>18</sup> are experimentally accessible using scattering methods. Here, neutron scattering measurements are made to obtain the average molecular structure and

to sub-picosecond time range. A schematic depiction of the local structure of water is shown in Figure 1, noting the approximate atomic distances to near neighbor molecules of liquid water<sup>1, 4-7</sup>. This descriptions of the average structure of the fluctuating tetrahedral network in liquid water can be experimentally obtained at the molecular/atomic scale using scattering methods. The early X-ray studies of Bernal<sup>5</sup> provide a surprisingly accurate understanding of the molecular spacing and tetrahedral organization of water molecules within the liquid. This understanding has been significantly refined using neutron diffraction<sup>4, 6, 7</sup> which adds detail about hydrogen positions explicitly, as neutrons scatter strongly from both hydrogen (deuterium) and oxygen<sup>33</sup>, while X-rays scatter predominately from oxygen. In Figure 1, the static structure factor (the experimental quantity we obtain from elastic scattering experiments) of water/D<sub>2</sub>O at 300K from both neutron and X-ray scattering is shown (X-ray data from Hura et al.<sup>1</sup>), in addition to pair distribution functions extracted from scattering measurements from the literature<sup>4</sup>.

This structural picture is relevant in order to define which atomic/molecular correlations contribute to the coherent inelastic neutron scattering in our experimental window. This is defined by the scattering wave vector,  $q$ , between 0.2 to 2.0 Å<sup>-1</sup>; and specifically around the  $q$ -range of first sharp diffraction peak of D<sub>2</sub>O,  $q > 1.3$  Å<sup>-1</sup>. This equates to real space distances less than ~4.5 Å, corresponding to  $d < 2\pi/q$ , and greater than ~3 Å, as defined by our instrumental constrains of  $q < 2.0$  Å<sup>-1</sup>. Within this range there are relevant pair-distances of all atom pairs; O-O correlations ~2.8 Å, and second shell correlations around 4.2 Å, D-D correlations ~4 Å, and O-D correlations ~3.5 Å. Note, many of the smallest correlations such as the O-D spacing of the hydrogen (deuterium) bond at ~1.8 Å are outside of the range of the  $q$ -range of the inelastic measurements presented here. This also illustrates a key difference with respect to X-ray

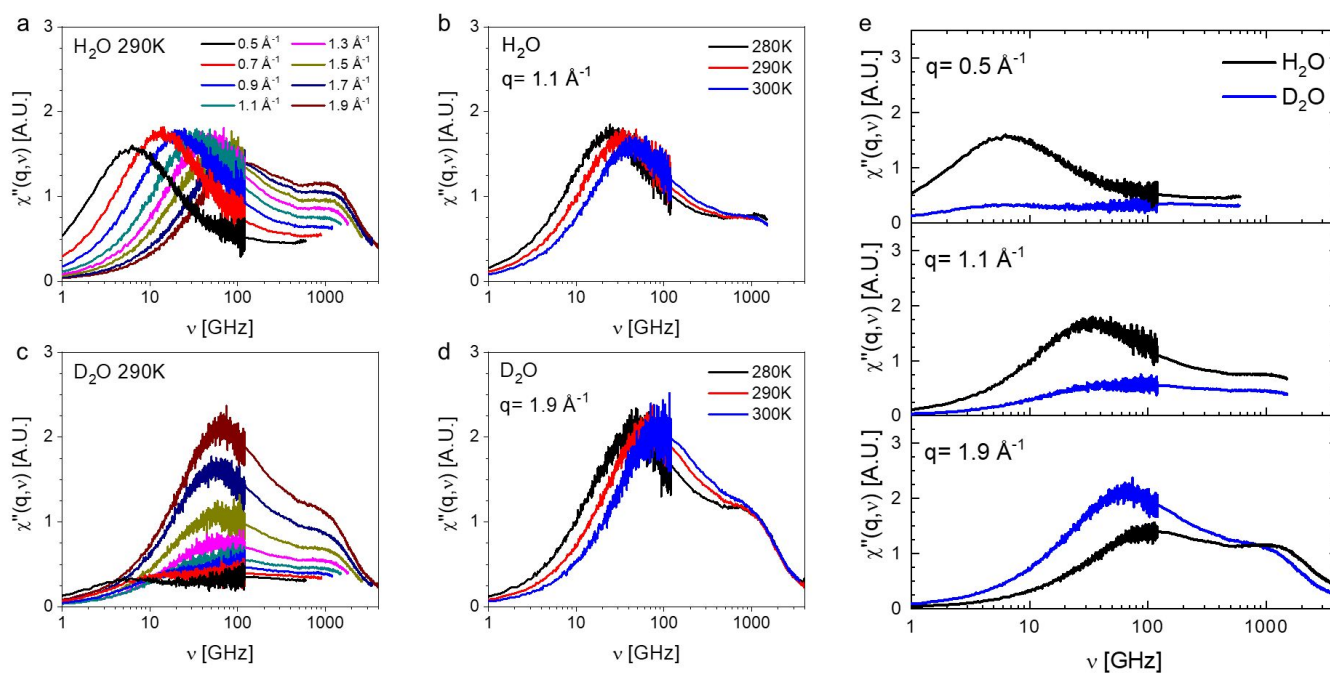


**Figure 2.** Inelastic neutron scattering spectra of H<sub>2</sub>O and D<sub>2</sub>O at 290 K presented in the susceptibility formalism. Spectra of (a) H<sub>2</sub>O and (c) D<sub>2</sub>O for a range of  $q$ -values. (a) Illustrates the strong  $q$ -dependence of the incoherent scattering feature; while (d) demonstrates the  $q$ -independence of the coherent scattering feature with a maximum intensity at the length scale of the first sharp diffraction peak. (b) and (d) show the temperature dependence of the scattering, with the peak positions shifting to higher frequency with increasing temperature. (e) directly compares H<sub>2</sub>O and D<sub>2</sub>O spectra at various  $q$ -values.

measurements which reflect only the O-O correlations between neighboring molecules; indeed, this is why the shape of the first sharp diffraction peak in Figure 1 differs between the two methods.

The molecular scale relaxations of water have been studied extensively by simulation<sup>14, 25, 34</sup> and many experimental techniques such as: vibrational spectroscopy<sup>35-38</sup>, terahertz spectroscopy<sup>39</sup>, optical Kerr-effect spectroscopy<sup>40</sup>, X-ray scattering<sup>2</sup>, and neutron scattering<sup>3, 41</sup>. Each technique has specific advantages and distinct time and length scales associated with the measurement; with inelastic neutron scattering perhaps the most powerful of these methods over the sub nanometer length-scale and nanosecond to sub-picosecond time-scale. Beyond the length-scale resolved spectroscopic description of technique can probe both the self-motion of hydrogen atoms within water, as well as resolving the atomic pair lifetimes associated with the water network; depending upon the isotopic variants of water used<sup>33</sup>. Hydrogen, <sup>1</sup>H (or simply H), has a large incoherent scattering cross-section. This means that we observe predominately incoherent inelastic neutron scattering from H<sub>2</sub>O, reflecting the motions of individual hydrogen atoms and the associated length scale of motion. Whereas <sup>2</sup>H (or D) has a small incoherent cross-section and larger coherent cross-section, meaning that scattering from D<sub>2</sub>O primarily reflects the lifetime of spatial correlations between nearby atoms.

The inelastic neutron scattering spectra of H<sub>2</sub>O and D<sub>2</sub>O were measured at 280 K, 290 K and 300 K. In this case, we obtain a dynamic range of up to three decades in frequency, ~1 GHz to greater than 1,000 GHz, for probe lengths ranging from ~3 Å to

3 nm ( $q$  from 0.2 Å<sup>-1</sup> to 2 Å<sup>-1</sup>). The stitched inelastic neutron scattering spectra of H<sub>2</sub>O and D<sub>2</sub>O at 300 K are shown in Figure 2 as a function of  $q$  and  $\nu$ . The observed quantity from these experiments is the dynamic structure factor  $S(q, E)$ , where  $E$  is energy transfer, and  $q$  is the scattering wave vector. The energy axis is converted to frequency,  $\nu$ , and  $S(q, E)$  transformed into the susceptibility formalism,  $\chi''(q, \nu)$ , as described in the methods and seen in Figure 2. This formalism is advantageous for several reasons, such as the emphasis of the inelastic/quasielastic regions of the spectra and the fact that well-separated dynamical processes appear as distinct maxima. The scattering spectra of H<sub>2</sub>O in this frequency/probe length range are dominated by the incoherent contribution, meaning that these spectra reflect the distribution of times needed for individual <sup>1</sup>H atoms to move a defined distance relative to their initial position. A strong  $q$ -dependence is observed in the main feature of the scattering; with the peak maxima trending to higher frequency with increasing  $q$  (or shorter distances).

The inelastic scattering from D<sub>2</sub>O differs substantially from that of H<sub>2</sub>O based on a simple visual inspection of the scattering data in Figure 2, with the strongest spectral feature emerging around 100 GHz only for the larger values of  $q$ , closely following that of the static structure factor. This is consistent with the notion that the scattering observed from D<sub>2</sub>O is primarily coherent scattering in this regime, reflecting the distribution of atom pair lifetimes, with a minor incoherent contribution superimposed that parallels the dynamics of H<sub>2</sub>O. This incoherent contribution is most apparent as a weak,  $q$ -dependent, feature visible at low  $q$ . A direct comparison of the spectra of H<sub>2</sub>O and D<sub>2</sub>O at a common  $q$  value highlights these differences in Figure 2. At low

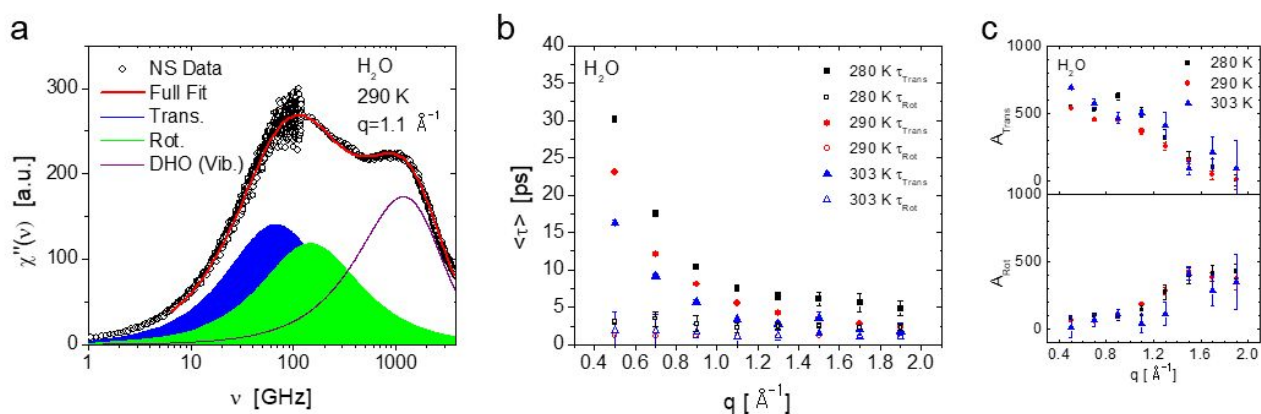


**Figure 3.** Fitting of the predominantly inelastic neutron scattering spectra of H<sub>2</sub>O. **(a)** A two-Debye model was used with the inclusion of a damped harmonic oscillator to account for the vibrational modes at high frequency. This treatment is a frequency domain analog to that performed by Teixeira and coworkers<sup>3</sup> and yielded comparable results. **(b)** Relaxation times for the two Debye functions corresponding to translational,  $\tau_{\text{trans}}$ , and rotational,  $\tau_{\text{rot}}$ , motions. **(c)** The relative amplitudes of the two Debye functions. Note the translational contribution dominates the amplitude of scattering at low- $q$  and the rotational component is larger at high- $q$ .

$q$  ( $q = 0.7 \text{ \AA}^{-1}$  for instance), there is a clear parallel between the incoherent feature in H<sub>2</sub>O and the weak incoherent feature observed in D<sub>2</sub>O. Though, it should be noted that the feature for D<sub>2</sub>O appears at lower frequency in agreement with the lower self-diffusion coefficient of D<sub>2</sub>O<sup>42</sup>.

A quantitative description of the molecular motions has been obtained from modeling these spectra. Beginning with H<sub>2</sub>O, a description can be obtained using three distinct contributions<sup>3</sup>; a Debye function to represent the translational motions (analogous to a Lorentzian distribution in the intensity formalism), another Debye function to represent the rotational motions, and a damped harmonic oscillator (DHO) to account for the intermolecular collective modes of H-bond bending motions at  $\sim 1500 \text{ GHz}$ <sup>43-45</sup>. The DHO is given by the relation;  $\chi_{DHO}'' = \mathcal{I}m\{\Delta_{DHO}\omega_0^2[\omega^2 - \omega_0^2 - i\omega\Gamma]^{-1}\}$  (4), where  $\omega_0$  is the position,  $\Gamma$  is the width, and  $\Delta_{DHO}$  is the amplitude.

The results of this data treatment, shown in Figure 3, produce a close agreement with literature<sup>3</sup>; with the translational relaxation times,  $\tau_{\text{trans}}$ , decreasing with a near  $q^2$  dependence in agreement with a jump diffusion motions and the rotational relaxation times,  $\tau_{\text{rot}}$ , not changing greatly with  $q$ . The relative amplitudes of these two contributions are inversely related, with the translational contribution dominant at longer length scales (low- $q$ ) and the rotational contribution dominating at shorter length scales (high- $q$ ). The observed rotational relaxation time at  $q=1.9 \text{ \AA}^{-1}$  was found to vary from 1-2 ps over the range of 280K-303K; while the translational motions occurring on this length scale were somewhat slower and varied with  $q$  and temperature, both in good agreement with prior work<sup>3</sup>.

The preceding data treatment decomposes water dynamics into pure translational and rotational motions for the purpose of simplifying the nature of the motions. Moreover, this treatment implies a decoupling which is not the complete picture of water motions<sup>34</sup>. Translation and rotation are actually coupled over the length scales probed in this experiment, weakly at low  $q$  ( $\leq 1$

$\text{\AA}^{-1}$ ) and strongly at high  $q$  ( $>1\text{\AA}^{-1}$ )<sup>46</sup>. The extended jump model for water reorientation proposed by Laage and Hynes<sup>34</sup> suggests a picture of this coupled local reorientation occurring on the order of 4 ps, via a concerted mechanism with a water molecule breaking its hydrogen bond with an over-coordinated first shell neighbor, and forming a new hydrogen bond with an uncoordinated water molecule in the second shell; undergoing a rapid  $\sim 60^\circ$  angular rotation and changing the distance between the initial oxygen-oxygen pair from  $\sim 2.8 \text{ \AA}$  in the first shell to  $\sim 4.2 \text{ \AA}$  in the second shell. Indeed, it is sometimes convenient in this experimental window to treat H<sub>2</sub>O inelastic spectra using a single Cole-Davidson function, analogous to a stretched exponential decay in the time domain. The consistency of this approach is illustrated in Perticaroli et al.<sup>47</sup>, with a reported timescale transitioning smoothly between the times reported in the decoupled model, and the amplitude of the coupled feature closely resembling the sum of the decoupled components. The approach is especially useful to simplify the treatment of two separate water populations (bulk and interfacial) when it is practical to replicate the incoherent contribution of water dynamics via a single functional form; such as bulk and hydration in analyses of water in the presence of solutes or surfaces<sup>47-50</sup>. Another useful approach to the fitting of the water spectra is the relaxing cage model<sup>51-53</sup> which has proven valuable to some investigators seeking to understand structural dynamics of water from the perspective of mode coupling theory<sup>54</sup> or within a continuous random walk model<sup>51</sup>. To quantify the timescale of the observed scattering for D<sub>2</sub>O – physically the superposition of atom pair lifetimes at the length scale of the scattering wave vector - a fitting procedure was used where the coherent scattering is represented as an additional Debye function, with the vibrational motions at high frequency again represented with a DHO, and the incoherent contribution represented by two Debye functions as seen in the case of H<sub>2</sub>O. The two incoherent contributions are clearly minor contributions at high  $q$  and can be constrained in the fitting process by fixing the respective time constants based on the

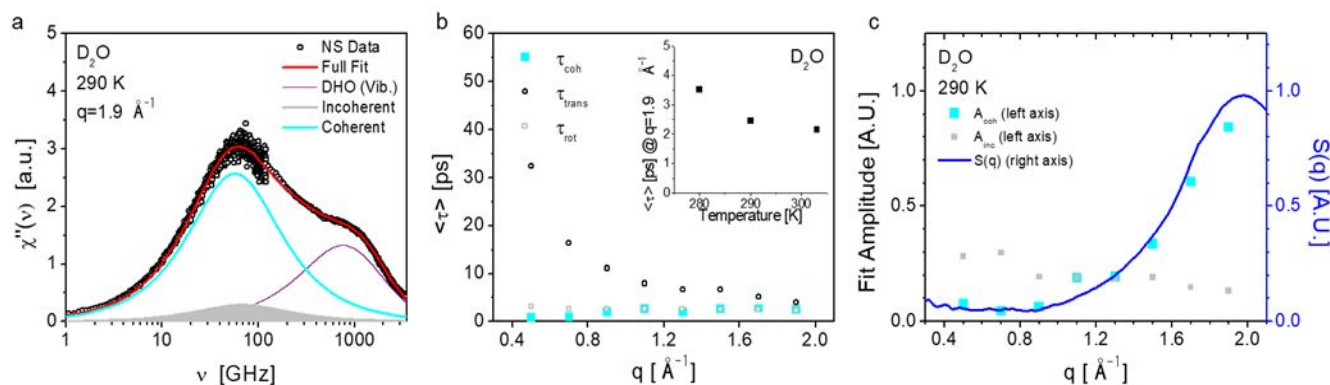


**Figure 4.** (a) Fitting of the inelastic neutron scattering spectra from D<sub>2</sub>O. The fit is comprised of two Debye functions representing the incoherent scattering (shown together in gray), an additional Debye function representing coherent inelastic scattering, and a DHO representing the vibrational component. (b) The average relaxation time from the coherent contribution was observed at  $\sim 2$  ps. (c) The amplitude of the coherent component (cyan square) clearly follows the static structure factor of D<sub>2</sub>O, supporting the notion that this feature is coherent in origin – reflecting the average lifetime of correlations making up this structural feature; namely, O-O, D-O, and D-D correlations noted in Figure 1.

observations from H<sub>2</sub>O and the observed diffusion constants in literature<sup>42</sup>; as well as fixing the amplitude of the incoherent contributions at high  $q$  based upon observed amplitude of the incoherent translational feature at low  $q$  in D<sub>2</sub>O where the incoherent feature is apparent and can be scaled to that observed for H<sub>2</sub>O.

The amplitude of the observed coherent feature emerges in line with the first sharp diffraction peak at  $q > 1.3 \text{ \AA}^{-1}$ , corresponding to real space atomic correlations of 2.5 to 4.2 Å. There is a clear amplitude agreement with the static structure factor, confirming the coherent nature of the observed feature. The observed time scale at which these correlations are broken varied between  $\sim 1$  and  $\sim 2$  ps over the 280K to 303K temperature range, very much in line with what could be expected by obtaining the peak maximum. The observed timeframe agrees with the slower mode reported by Iwashita et al.<sup>2</sup> using inelastic x-ray scattering on H<sub>2</sub>O and was assigned to the local molecular rearrangements between the second shell oxygen atoms. Here, the large coherent scattering length of both deuterium and oxygen mean that the correlations observed in this study include D-D and O-D, in addition to O-O. Despite of well-known differences in the structure and hydrogen/deuterium bond between H<sub>2</sub>O and D<sub>2</sub>O<sup>55</sup>, the observation of a coincidence in approximate timescales for the molecular rotation of water, and the disruption of local structure seen in the first sharp diffraction peak of D<sub>2</sub>O clearly identifies the 1-2 ps timeframe as relevant to the structural relaxation controlling bulk viscosity. Both the bulk viscosity,  $\zeta$ , and the bulk modulus,  $K$ , can be obtained experimentally from Brillouin scattering. Brillouin scattering is an inelastic light scattering technique which can be used to assess the sound velocity. The observed spectra, Figure 5 (a-d), were collected as observed intensity,  $I_B(\nu)$ , as a function of frequency,  $\nu$ . The longitudinal mode apparent in the observed spectra can be modelled using a damped harmonic oscillator model<sup>56, 57</sup>, (DHO);

$$I_B(\nu) = A \frac{\Gamma_L \Omega_L}{(\nu^2 - \Omega_L^2)^2 + (\Gamma_L \nu)^2} + y_0 \quad (5),$$

where  $\Omega_L$  is the oscillator frequency and  $\Gamma_L$  is the full width at half-maximum of the spectral feature.  $A$  and  $y_0$  are the

amplitude and background. The spectra are collected on both the Stokes and anti-Stokes regions. The fit parameters,  $\Omega_L$  and  $\Gamma_L$  are used to obtain the longitudinal sound velocity,  $c_L$ , the bulk viscosity,  $\zeta$ , and the bulk modulus,  $K$ . In the backscattering geometry, the sound velocity can be calculated as;

$$c_L = \frac{\Omega_L \lambda}{2n}, \quad (6),$$

where  $\lambda$  is the incident wavelength and  $n$  is the refractive index. The observed values are in close agreement with prior reported values.<sup>58-60</sup> The bulk modulus,  $K$ , can be calculated using the calculated  $c_L$ , the constant volume and constant pressure heat capacities,  $C_V$  and  $C_P$ , and the density,  $\rho$ , using;

$$K = c_L^2 \rho \frac{C_V}{C_P}, \quad (7).$$

The bulk viscosity is obtained from the damping of the longitudinal mode observed here as the linewidth. For the case of H<sub>2</sub>O and D<sub>2</sub>O in the temperature range considered here, the ratio of constant volume to constant pressure specific heat is close to unity, so contributions from thermal conductivity can be neglected, resulting in the simplified relation;

$$\zeta = \frac{\rho c_L^2 \Gamma_L}{4\pi^2 \Omega_b^2} - \frac{4}{3}\mu, \quad (8).$$

The relevant time scale for the molecular motions governing the bulk viscosity of water can now be estimated using the relation  $\zeta/K = \tau_b$ . All calculated parameters have been summarized in Figure 5 as a function of temperature. The sound velocity is seen to increase with temperature, and as expected for both H<sub>2</sub>O and D<sub>2</sub>O; the bulk modulus goes through a maximum above the temperature range considered here.

The resulting time scales of molecular relaxation are found on the order of  $\sim 1$  to 2 ps, significantly slower than the motions governing the shear behavior of water as seen recently by Iwashita et al.<sup>2</sup> That study investigated the timeframe of local molecular rearrangements in water using a real-space analysis to extract the van Hove<sup>61</sup> function from inelastic x-ray scattering experiments. This allowed the authors to follow the time and space correlations of the oxygen atoms, showing the loss of correlation between oxygen atoms of neighboring molecules. The observations seem to identify a distinct decay time for the correlations of the neighbouring oxygen atoms; providing a dynamical time scale comparable to the predicted Maxwell relaxation time from shear viscosity for liquid water below the

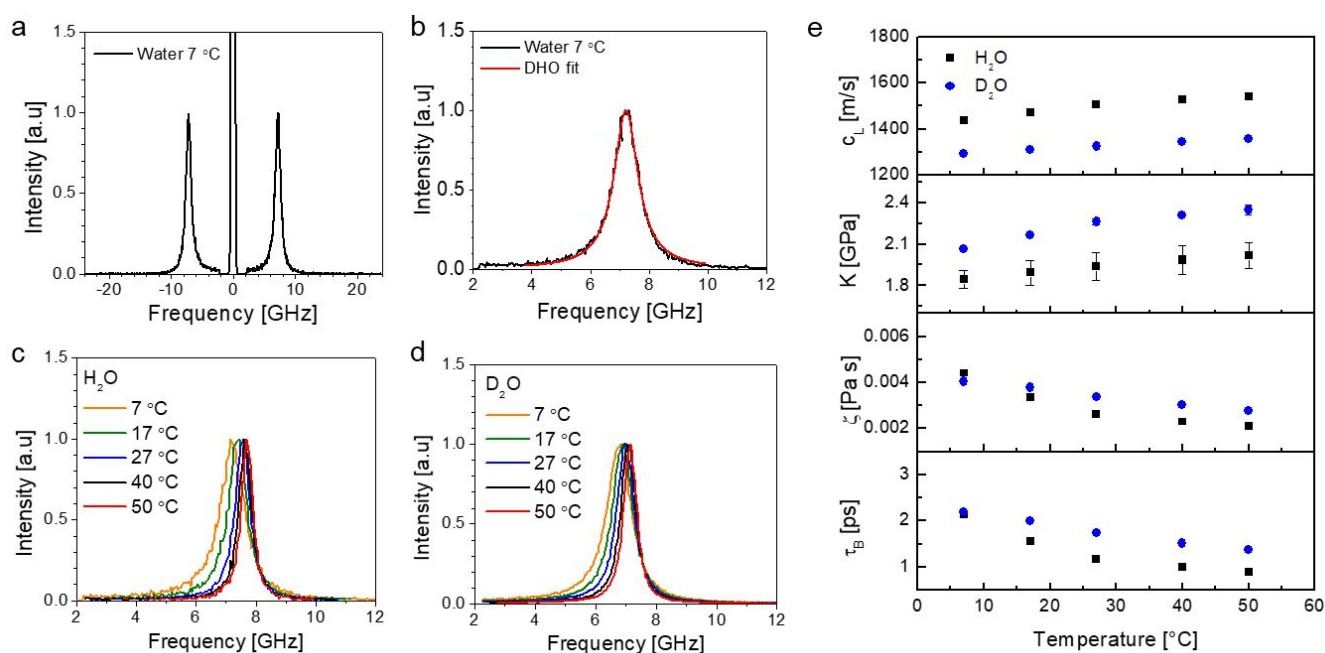


**Figure 5.** Brillouin scattering measurements can be used to measure the longitudinal sound velocity,  $c_L$ , bulk modulus,  $K$ , bulk viscosity,  $\zeta$ , and associated relaxation time,  $\tau_B$ . **(a)** Representative spectrum from  $\text{H}_2\text{O}$  showing the symmetric Stokes and anti-Stokes features. **(b)** The spectra can be described as a damped harmonic oscillator (DHO), extracting the oscillator frequency and the full-width at the half-maximum of the feature. **(c)** and **(d)** show the temperature dependences of the spectra for both  $\text{H}_2\text{O}$  and  $\text{D}_2\text{O}$ . **(e)** Computed properties obtained as a function of temperature, identifying the relevant timescale of molecular relaxation for bulk viscosity.

viscosity crossover temperature  $\sim 60^\circ\text{C}$ <sup>28</sup>, in potential agreement with ultrafast spectroscopy<sup>37</sup>.

The dynamic hydrogen bond network in water constantly changes connectivity in a complex dance of this attractive interaction and rapid molecular motions. The breaking of a single hydrogen bond is associated with local reorientations of water molecules on the sub-picosecond timescale<sup>25</sup>, which appear to provide sufficient molecular flexibility to relieve the molecular scale shear stress within the network. Moreover, the rapid motions associated with shear viscosity are consistent with the translational jump timescale predicted from a jump diffusional model<sup>2, 3, 62</sup>. This makes a logical and expected connection of translational diffusion and shear viscosity.

Alternately referred to as the volume viscosity or dilatational viscosity; the bulk viscosity describes the viscous resistance to volume change. It is reasonable then to consider that the timescale of microscopic density fluctuations within the material will be relevant. Indeed, coherent neutron scattering observations of  $\text{D}_2\text{O}$  at the length scale of the first sharp diffraction peak reflect a weighted average lifetime of the correlations contributing to the structural peak, providing an experimental description of the lifetime of microscopic density fluctuations at 1-2 ps, coinciding closely with the bulk modulus relaxation time.

The further coincidence of rotational dynamics of water identifies a timescale of molecular motions as well. As we have emphasized earlier, the assumption of pure rotational dynamics made in this analysis is based on a common<sup>41</sup> and classical approach<sup>3</sup> of analytical simplicity and does not reflect recent development such as the extended jump model for water

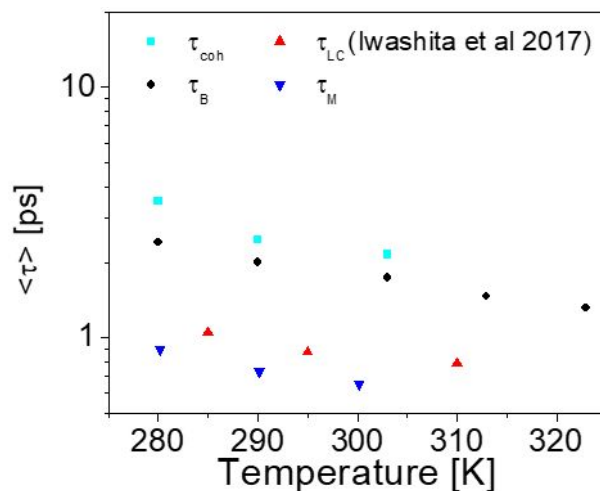


**Figure 6.** Comparison of rheological timescales for bulk and shear viscosity. Here,  $\tau_{\text{coh}}$  and  $\tau_B$  are reported for  $\text{D}_2\text{O}$  while  $\tau_M$  and  $\tau_{\text{LC}}$  are reported from Iwashita et al.<sup>2</sup> for  $\text{H}_2\text{O}$ . This figure illustrates that rapid fluctuations on the sub-picosecond timescale are sufficient to relieve local shear stress, whilst slower motions related to water rotation control reset structure on the order of the first sharp diffraction peak and limit the viscous response to local volume changes.

reorientation proposed by Laage and Hynes<sup>34</sup>. As noted above, a more generic localized motion within a cage, or local energy basin, is a common alternate interpretation of the observed proton motions in incoherent inelastic neutron scattering. This concept is extensively developed by Qvist, Schober and Halle<sup>51</sup> and leads into a number of recent analyses of water

properties<sup>53</sup>. The reader should be clear that many more models of water dynamics are proposed than are discussed here, however. Regardless of any existing debate about the exact nature of these motions, it is clear that protons in water are moving in a highly localized ( $<1\text{\AA}$ ) fashion on the timescale of 1-2 ps, and that these motions coincide with the bulk viscous response.

## Conclusions

As can be seen in Figure 6, the timescale observed for bulk viscosity, on the order of 1-2 ps, compares favorably to the structural reorganization occurring on the order of 1-2 ps in  $\text{D}_2\text{O}$  at temperatures ranging from 280 K to 303K. The approach of Hall<sup>32</sup> to the calculation of a Maxwell time for bulk viscosity predicts a timescale for molecular rotations or localized motions to act as density fluctuations which permit a reset of the local volume to conform to the local pressure. This is in parallel to shear viscosity, where the molecular configurations reset the local stress tensor. The first sharp diffraction peak reflects a collection of atomic correlations resulting from the local molecular spacing, and it is logical that the lifetime of the correlations is intimately connected to the bulk viscous response. The rotation of the water molecule can be understood to disrupt many of the atomic correlations within liquid water. Specifically, considering those just noted as comprising the first sharp diffraction peak for neutrons. O-H, O-O, and H-H atom pairs in Figure 1. All would all disrupted by a 60-degree rotation of the water molecule, consistent with the mechanism of rotation and coincident with the timescale identified as resetting of the local volume.

The implications of this work are twofold. Firstly, we have illustrated the fundamental molecular timescale of bulk viscosity in liquid water, and correlating it to a specific molecular spacing and relaxation using light and neutron scattering methods. The results illustrate a connection between rotational motions on the length scale of the first sharp diffraction peak for neutrons; and the viscous response to rapid volume changes. Secondly, we show that the motions associated with the bulk viscous response occur two to three times slower than those associated with the shear viscous response; with the connectivity of the fluctuating hydrogen bond network varying faster than the local density fluctuations.

## Methods

Neutron diffraction measurements were conducted at the Nanoscale Ordered Materials Diffractometer (NOMAD)<sup>63</sup> at the Spallation Neutron Source, Oak Ridge National Laboratory.  $\text{D}_2\text{O}$  samples were measured in 2.5 mm diameter quartz capillary tubes at 23°C. Diffraction spectra were obtained in the  $q$  range from 0.2 to 50  $\text{\AA}^{-1}$  and were normalized against a solid vanadium rod. The the capillary background was subtracted from the data. Scattering data from all detector banks were combined to improve the counting statistics in the low  $q$  region.

The inelastic neutron scattering spectra of  $\text{H}_2\text{O}$  and  $\text{D}_2\text{O}$  were measured at 280 K, 290 K and 300 K, using two spectrometers, BASIS<sup>64</sup> and CNCS<sup>65</sup> at the Spallation Neutron Source, Oak Ridge National Laboratory, Tennessee, USA. BASIS is a backscattering spectrometer with a resolution of  $\sim 3\mu\text{eV}$ , it was operated in an asymmetric, frame-skipping mode with incident wavelength of 6.15 $\text{\AA}$ . CNCS is a time of flight spectrometer which was operated at an incident wavelength of 3  $\text{\AA}$ , with an instrumental resolution of approximately 50  $\mu\text{eV}$ . The energy change axis of the resulting spectra is converted to frequency,  $\nu$ . These spectrometers were utilized in a configuration which results in an overlapping  $q$ - $\nu$  range, allowing the datasets to be combined. The observed spectra were first processed into slices along the energy axis, binning the data at defined  $q$ -values common to both instruments, and then transformed into the susceptibility formalism,  $\chi''(q,\nu)$ , as seen in Figure 2, according to the relation;  $\chi''(q,\nu) \propto S(q,\nu)/n_B(\nu)$  (9),

$$n_B(\nu) = [\exp(h\nu/kT) - 1]^{-1} \quad (10),$$

where  $S(q,\nu)$  is the measured dynamic structure factor and; is the Bose occupation number<sup>66</sup>. This formalism is advantageous for several reasons, such as the emphasis of the inelastic/quasielastic regions of the spectra and the fact that well-separated dynamical processes appear as distinct maxima. The latter point facilitates the stitching of neutron data from different spectrometers at common  $q$ -values to achieve a larger dynamic range than possible from a single spectrometer. In this case, we obtain a dynamic range of up to three decades in frequency,  $\sim 1$  GHz to greater than 1,000 GHz, for probe lengths ranging from  $\sim 3$   $\text{\AA}$  to 3 nm ( $q$  from 0.2  $\text{\AA}^{-1}$  to 2  $\text{\AA}^{-1}$ ).

Brillouin scattering measurements were performed in a polarized, backscattering configuration using a Sandercock tandem Fabry-Perot interferometer with a 532 nm single-mode solid state laser. A 6mm mirror separation was used, giving a free spectral range of 24 GHz. 300  $\mu\text{L}$  samples of  $\text{H}_2\text{O}$  and  $\text{D}_2\text{O}$  were sealed and placed in a Linkam temperature control cell. The samples were allowed to equilibrate for a minimum of 30 minutes at each temperature prior to measurement. Spectra were collected over approximately 60 minutes.

## Conflicts of interest

The authors have no conflicts to declare.

## Acknowledgements

This work was supported by the U.S. National Science Foundation (CBET- 1836556) and the University of Cincinnati. Research at Oak Ridge National Laboratory's Spallation Neutron Source was sponsored by the Scientific User Facilities Division, Office of Basic Energy Sciences, DOE. Oak Ridge National Laboratory facilities are sponsored by UT-Battelle, LLC, for the U.S. Department of Energy under Contract No. DEAC0500OR22725.

## Notes and references

1. G. Hura, D. Russo, R. M. Glaeser, T. Head-Gordon, M. Krack and M. Parrinello, *Physical Chemistry Chemical Physics*, 2003, **5**, 1981-1991.
2. T. Iwashita, B. Wu, W.-R. Chen, S. Tsutsui, A. Q. Baron and T. Egami, *Science advances*, 2017, **3**, e1603079.
3. J. Teixeira, M. C. Bellissent-Funel, S. H. Chen and A. J. Dianoux, *Physical Review A*, 1985, **31**, 1913-1917.
4. A. Soper and M. Phillips, *Chemical Physics*, 1986, **107**, 47-60.
5. J. D. Bernal and R. H. Fowler, *The Journal of Chemical Physics*, 1933, **1**, 515-548.
6. A. Soper, *Chemical Physics*, 2000, **258**, 121-137.
7. A. Zeidler, P. S. Salmon, H. E. Fischer, J. C. Neufeind, J. M. Simonson and T. E. Markland, *Journal of Physics: Condensed Matter*, 2012, **24**, 284126.
8. P. H. Poole, F. Sciortino, U. Essmann and H. E. Stanley, *Nature*, 1992, **360**, 324.
9. P. Bridgman, *The Journal of Chemical Physics*, 1935, **3**, 597-605.
10. M. W. Mahoney and W. L. Jorgensen, *The Journal of Chemical Physics*, 2000, **112**, 8910-8922.
11. G. S. Kell, *Journal of Chemical and Engineering Data*, 1975, **20**, 97-105.
12. J. R. Errington and P. G. Debenedetti, *Nature*, 2001, **409**, 318.
13. E. Sanz, C. Vega, J. Abascal and L. MacDowell, *Physical review letters*, 2004, **92**, 255701.
14. F. H. Stillinger and A. Rahman, *The Journal of Chemical Physics*, 1974, **60**, 1545-1557.
15. N. Hirai and H. Eyring, *Journal of Applied Physics*, 1958, **29**, 810-816.
16. F. Jaeger, O. K. Matar and E. A. Müller, *The Journal of Chemical Physics*, 2018, **148**, 174504.
17. J. Copley, SW Lovesey, *Rep. Prog. Phys.*, 1975, **38**, 461.
18. P. G. De Gennes, *Physica*, 1959, **25**, 825-839.
19. E. Thiele, *The Journal of Chemical Physics*, 1963, **39**, 474-479.
20. M. Wertheim, *Physical Review Letters*, 1963, **10**, 321.
21. J. Irving and J. G. Kirkwood, *The Journal of chemical physics*, 1950, **18**, 817-829.
22. L. Verlet, *Physical review*, 1967, **159**, 98.
23. J. Nicolas, K. Gubbins, W. Streett and D. Tildesley, *Molecular Physics*, 1979, **37**, 1429-1454.
24. W.-T. Ashurst and W. Hoover, *Physical Review A*, 1975, **11**, 658.
25. A. Luzar and D. Chandler, *Nature*, 1996, **379**, 55.
26. G. G. Stokes, *Transactions of the Cambridge Philosophical Society*, 1880, **8**.
27. J. C. Maxwell, *Philosophical transactions of the Royal Society of London*, 1867, **157**, 49-88.
28. T. Egami, *Quantum Beam Science*, 2018, **2**, 22.
29. P. M. Gary and J. E. Denis, *Statistical Mechanics of Nonequilibrium Liquids*, ANU Press, Canberra, 2007.
30. J.-P. Hansen and I. R. McDonald, *Theory of simple liquids*, Elsevier, 1990.
31. T. Egami and D. Srolovitz, *Journal of Physics F: Metal Physics*, 1982, **12**, 2141.
32. L. Hall, *Physical Review*, 1948, **73**, 775.
33. V. F. Sears, *Neutron news*, 1992, **3**, 26-37.
34. D. Laage and J. T. Hynes, *Science*, 2006, **311**, 832-835.
35. a. Woutersen, U. Emmerichs and H. Bakker, *Science*, 1997, **278**, 658-660.
36. J. B. Asbury, T. Steinel, C. Stromberg, S. Corcelli, C. Lawrence, J. Skinner and M. Fayer, *The Journal of Physical Chemistry A*, 2004, **108**, 1107-1119.
37. C. Fecko, J. Eaves, J. Loparo, A. Tokmakoff and P. Geissler, *Science*, 2003, **301**, 1698-1702.
38. F. Perakis, L. De Marco, A. Shalit, F. Tang, Z. R. Kann, T. D. Kühne, R. Torre, M. Bonn and Y. Nagata, *Chemical Reviews*, 2016, **116**, 7590-7607.
39. C. Rønne, P.-O. Åstrand and S. R. Keiding, *Physical review letters*, 1999, **82**, 2888.
40. K. Winkler, J. Lindner, H. Bürsing and P. Vöhringer, *The Journal of Chemical Physics*, 2000, **113**, 4674-4682.
41. K. Amann-Winkel, M.-C. Bellissent-Funel, L. E. Bove, T. Loerting, A. Nilsson, A. Paciaroni, D. Schlesinger and L. Skinner, *Chemical Reviews*, 2016, **116**, 7570-7589.
42. R. Mills, *The Journal of Physical Chemistry*, 1973, **77**, 685-688.
43. S. Perticaroli, L. Comez, M. Paolantoni, P. Sassi, L. Lupi, D. Fioretto, A. Paciaroni and A. Morresi, *The Journal of Physical Chemistry B*, 2010, **114**, 8262-8269.
44. S. Perticaroli, L. Comez, M. Paolantoni, P. Sassi, A. Morresi and D. Fioretto, *Journal of the American Chemical Society*, 2011, **133**, 12063-12068.
45. M. Settles and W. Doster, *Faraday Discussions*, 1996, **103**, 269-279.
46. D. Di Cola, A. Deriu, M. Sampoli and A. Torcini, *The Journal of chemical physics*, 1996, **104**, 4223-4232.
47. S. Perticaroli, G. Ehlers, C. B. Stanley, E. Mamontov, H. O'Neill, Q. Zhang, X. Cheng, D. A. Myles, J. Katsaras and J. D. Nickels, *Journal of the American Chemical Society*, 2017, **139**, 1098-1105.
48. J. D. Nickels, J. Atkinson, E. Papp-Szabo, C. Stanley, S. O. Diallo, S. Perticaroli, B. Baylis, P. Mahon, G. Ehlers and J. Katsaras, *Biomacromolecules*, 2016, **17**, 735-743.
49. J. D. Nickels, H. O'Neill, L. Hong, M. Tyagi, G. Ehlers, K. L. Weiss, Q. Zhang, Z. Yi, E. Mamontov and J. C. Smith, *Biophysical journal*, 2012, **103**, 1566-1575.
50. P. B. Ishai, Z. Sobol, J. D. Nickels, A. L. Agapov and A. P. Sokolov, *Review of Scientific Instruments*, 2012, **83**, 083118.
51. J. Qvist, H. Schober and B. Halle, *The Journal of chemical physics*, 2011, **134**, 144508.
52. S. Chen, C. Liao, F. Sciortino, P. Gallo and P. Tartaglia, *Physical Review E*, 1999, **59**, 6708.
53. A. Arbe, P. M. De Molina, F. Alvarez, B. Frick and J. Colmenero, *Physical review letters*, 2016, **117**, 185501.
54. A. Arbe, J. Colmenero, F. Alvarez, M. Monkenbusch, D. Richter, B. Farago and B. Frick, *Physical Review E*, 2003, **67**, 051802.
55. A. Soper and C. Benmore, *Physical review letters*, 2008, **101**, 065502.
56. B. J. Berne and R. Pecora, *Dynamic light scattering: with applications to chemistry, biology, and physics*, Courier Corporation, 2000.
57. C. E. Bottani and D. Fioretto, *Advances in Physics: X*, 2018, **3**, 1467281.
58. J. Rouch, C. C. Lai and S. H. Chen, *The Journal of Chemical Physics*, 1976, **65**, 4016-4021.
59. J. Teixeira and J. Leblond, *Journal de Physique Lettres*, 1978, **39**, 83-85.
60. J. Xu, X. Ren, W. Gong, R. Dai and D. Liu, *Appl. Opt.*, 2003, **42**, 6704-6709.

## Journal Name

## ARTICLE

61. L. Van Hove, *Physical Review*, 1954, **95**, 249.
62. J. Teixeira, A. Luzar and S. Longeville, *Journal of Physics: Condensed Matter*, 2006, **18**, S2353.
63. J. Neufeind, M. Feygenson, J. Carruth, R. Hoffmann and K. K. Chiple, *Nuclear Instruments and Methods in Physics Research Section B: Beam Interactions with Materials and Atoms*, 2012, **287**, 68-75.
64. E. Mamontov and K. W. Herwig, *Review of Scientific Instruments*, 2011, **82**, 085109.
65. G. Ehlers, A. A. Podlesnyak, J. L. Niedziela, E. B. Iverson and P. E. Sokol, *Review of Scientific Instruments*, 2011, **82**, 085108.
66. M. Bee, *Biology and Materials Science*, Adam Hilger, Bristol, 1988, 193.